Functional Phenotype Flow Cytometry: On Chip Sorting of Individual Cells According to Responses to Stimuli

Nikiforov, Petar O ; Hejja, Beata ; Chahwan, Richard ; Soeller, Christian ; Gielen, Fabrice ; Chimerel, Catalin

DOI: https://doi.org/10.1002/adbi.202100220

ADVANCED BIOLOGY
www.advanced-bio.com

Functional Phenotype Flow Cytometry: On Chip Sorting of Individual Cells According to Responses to Stimuli

*Petar O. Nikiforov, Beata Hejja, Richard Chahwan, Christian Soeller, Fabrice Gielen, and Catalin Chimerel**

The ability to effectively separate and isolate biological cells into specific and well-defined subpopulations is crucial for the advancement of our understanding of cellular heterogeneity and its relevance to living systems. Here is described the development of the functional phenotype flow cytometer (FPFC), a new device designed to separate cells on the basis of their in situ real-time phenotypic responses to stimuli. The FPFC performs a cascade of cell processing steps on a microfluidic platform: introduces biological cells one at a time into a solution of a biological reagent that acts as a stimulus, incubates the cells with the stimulus solution in a flow, and sorts the cells into subpopulations according to their phenotypic responses to the provided stimulus. The presented implementation of the FPFC uses intracellular fluorescence as a readout, incubates cells for 75 s, and operates at a throughput of up to 4 cells min^{-1}—resulting in the profiling and sorting of hundreds of cells within a few hours. The design and operation of the FPFC are validated by sorting cells from the human Burkitt's lymphoma cancerous cell line Ramos on the basis of their response to activation of the B cell antigen receptor (BCR) by a targeted monoclonal antibody.

1. Introduction

The study and understanding of cellular heterogeneity are a fundamental aim of biology since the chemical, structural, and morphological differences between cells are related to their physiological functions.[1] During development, heterogeneity at the epigenome, transcriptome, and proteome levels allows cells with otherwise identical genomes to differentiate and assemble the functional tissues and organs of multicellular organisms. Cellular heterogeneity is also widely observed within populations of identically differentiated cells and can manifest itself as differences in the time-dependent phenotypic behavior of distinct cell subpopulations.[2,3]

Time-lapse fluorescence microscopy is a broadly adopted method used for investigating the heterogeneity of intracellular dynamics in living cells.[4,5] Live cell fluorescence dyes and genetically encoded fluorescence proteins are providing the means to analyze the dynamics of a wide range of intracellular processes under the fluorescence microscope. Alongside fluorescence microscopy, the emergence of single cell omic technologies has enabled the quantification of DNA, methylated DNA, RNA, protein or open chromatin nucleosome within individual cells.[6] Correlating single cell omics data with phenotypic measurements of intracellular dynamics would, in principle, allow an in-depth mapping between intracellular composition and function at the single cell level. Nevertheless, time-lapse fluorescence microscopy relies on cells being immobilized, usually as an adherent culture, and the successful harvesting of selected cells of interest for further investigation, for example by single cell omics, poses significant challenges and relies on the development of rapid, accurate and efficient cell sorting and manipulation technologies.

Currently used methods to isolate a cell following time-lapse fluorescence microscopy employ several strategies. Robotic cell picking, employs a suction pipette, to directly remove a cell of interest, from an adherent substrate, following a time-lapse fluorescence measurement. This methodology does not apply to cells that grow in suspension and has limited throughput since only the cells in the field of view constitute candidates for further analysis.[7] SPOTlight, employs light quenching of a fluorescent label, genetically expressed on the cell surface, to mark cells of interest.[8] The technology can be employed to mark a phenotype of interest following for example time-lapse fluorescence microscopy. Still the technology limits the analysis to the cells present in the field of view and can only work with adherent cell lines. Moreover, the use of the genetically encoded editable fluorescence label somewhat limits the throughput for primary cells lines. Alternative methods that work with non-adherent cell lines include μSCALE and SIFT.[9] These methods use compartments such us capillary arrays or droplets to identify single cells in space and time. However, confining cells

Dr. P. O. Nikiforov, B. Hejja, Prof. C. Soeller, Dr. F. Gielen, Dr. C. Chimerel
Living Systems Institute
University of Exeter
Stocker Road, Exeter EX4 4QD, UK
E-mail: C.Chimerel@exeter.ac.uk
Prof. R. Chahwan
Institute of Experimental Immunology
University of Zurich
Zurich 8057, Switzerland

The ORCID identification number(s) for the author(s) of this article can be found under https://doi.org/10.1002/adbi.202100220.

DOI: 10.1002/adbi.202100220

restricts the ability to alter the extracellular environment and freely study cellular responses, upon change in the extracellular environment, with time-lapse fluorescence microscopy.

On the other hand flow cytometry, laser capture microdissection (LCM),[10] immunomagnetic, microfluidic, limiting dilution and manual cell picking methods for the isolation of single cells have been previously described in the literature.[11] Fluorescence-assisted cell sorting (FACS) is currently the most widely used technology for the automated separation of cells according to fluorescent markers or light scattering properties.[11] In addition, a number of intelligent image-based cell isolation methods, which use high information-content fluorescence microscopy images, have been developed recently.[1,10] Furthermore, imaging flow cytometry (IFC)[12] has emerged as a technology, which combines traditional flow cytometry principles with advanced image acquisition and processing tools to achieve the morphometric characterization and isolation of single cells from large heterogeneous mixtures.[13]

In contrast with time-lapse fluorescence microscopy, FACS predominantly relies on single time point measurements and is therefore capable of separating cells only according to characteristics, which are intrinsic to the cells, or according to markers, which have been pre-loaded inside the cells or on the cell surface prior to sorting (e.g., fluorescent tags). Recently, Zhao et al reported a single-phase flow microfluidic cell sorter with a two-point fluorescence signal detection system, which was developed to assist with the directed evolution of Ca^{2+} sensors.[13] This technology uses a 3D focusing flow, which significantly improves throughput, nevertheless it employs two separate microscopes to take the fluorescence readings of cells at only two different time points along a microfluidic channel and suffers from significant errors in cell assignment. Here we report a novel approach, which allows observing single-cells at high throughput, at many time points, all using a single microscope, whilst enabling highly accurate cell registration. The new sorting device, which we term a functional phenotype flow cytometer (FPFC), is designed to sort biological cells according to their phenotypic responses to extracellular stimuli in flow with high fidelity. Our technology is based on a purpose designed microfluidic device and employs a single standard epifluorescence microscope to achieve fluorescence imaging of individual cells in flow at multiple time points. We validated the design and operation of the functional phenotype flow cytometer by demonstrating how Ramos cells can be separated according to their intracellular dynamic responses to stimulation of B-cell antigen receptors (BCRs) with a targeted monoclonal antibody. The human Burkitt lymphoma cell line Ramos, which originates from activated germinal center B cells, has been previously described as a suitable system for the study of biochemical mechanisms determining cell proliferation and programmed cell death.[15,16] Incubation of Ramos cells with a monoclonal antibody against BCR has been reported to result in elevation of the intracellular Ca^{2+} levels in a subpopulation of the cells.[17] The signaling cascade, which causes the increase of the intracellular Ca^{2+} concentration in Ramos as a result of antigen ligation of BCR has been extensively studied and described previously.[18,19] Here, the functional phenotype flow cytometer is used to observe the dynamic intracellular Ca^{2+} response of Ramos cells to treatment with anti-BCR monoclonal antibody and the subpopulation of cells reacting to the antibody is separated from a nonresponding population of cells.

2. Results

2.1. The Functional Phenotype Flow Cytometer

To assess intracellular dynamics in response to a stimulus, and separate cells of interest from a potentially heterogeneous cell mixture, the functional phenotype flow cytometer performs a series of three consecutive processes on a microfluidic chip: Firstly, the FPFC introduces biological cells one at time and at well-defined time points into a solution of a biological reagent (stimulus) of interest. Secondly, the FPFC incubates the cells with the stimulus solution in flow for a required period of time. Thirdly, the FPFC optically monitors the cellular responses in situ and sorts the cells into subpopulations according to their phenotypic responses to the provided stimulus. Similar to flow cytometry, an FPFC device without a sorting module is termed an "FPFC analyzer" and an FPFC device that incorporates a sorting module is referred to as an "FPFC sorter" (**Figure 1**B,C).

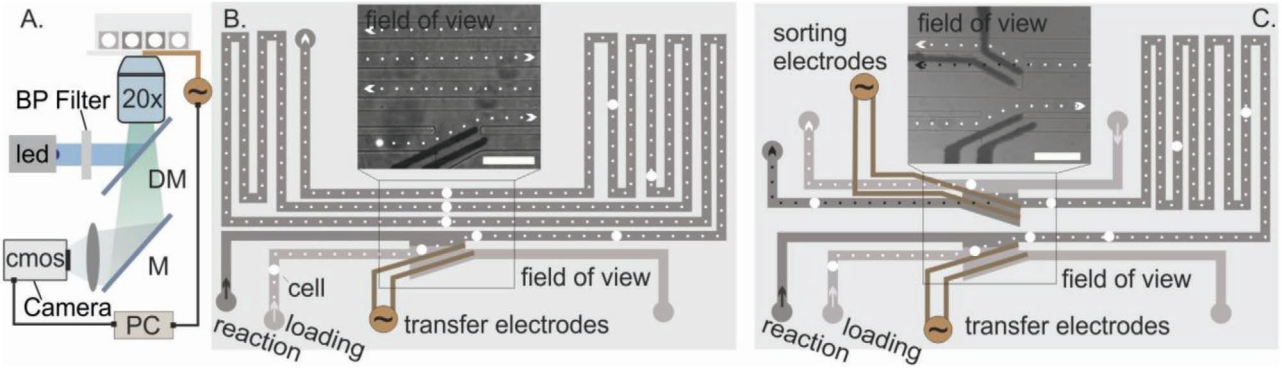

Figure 1. The functional phenotype flow cytometer (FPFC) analyzer and sorter modes. A) Schematic overview of the optical and electrical components of the FPFC (DM: dichroic mirror; M: mirror; BP: band pass filter). B) Schematics of a two-channel microfluidic FPFC analyzer and C) a three-channel FPFC sorter design. Cells inside the channels are represented as large white dots and possible cell paths are indicated by dotted lines with arrows indicating the direction of travel. Insets in (B) and (C) show the imaged sample areas in the center of the chips. The scale bars are 100 μm in length.

For both the FPFC analyzer and sorter to perform the cell manipulation processes highlighted above, a special microfluidic chip architecture coupled with a custom-built epifluorescence microscope and real-time cell tracking software have been developed.

2.1.1. Microfluidic Chip Function and Architecture

The microfluidic chip is designed to transfer cells between a loading microchannel and a reaction microchannel (Figure 1B,C). To achieve the inter-channel transfer, cells are introduced to the cell loading channel of the chip in their usual culturing media and a solution capable of delivering a stimulus is flown through the reaction channel. By means of dielectrophoresis[20] selected cells are transferred from the loading channel to the reaction channel (Figure 1B,C). This transfer process is possible since the loading channel and the reaction channel in the chip are fluidly connected via a 90 μm long inter-channel gap. Metal electrodes fitted to the inter-channel gaps (Figure 1B,C) are used to transfer the cells between the two channels. The laminar flows in the microchannels ensure well-defined interfacial boundaries at the inter-channel gaps with minimal mixing of liquids between two adjacent channels (Figure S8, Supporting Information). In addition, both the loading channel and the reaction channels are fitted with flow resistance loops. The loop that is part of the loading channel is about 90% shorter than the loop that is part of the reaction channel ensuring that no liquid from the loading channel flows into the reaction channel (Figure S3, Supporting Information). Since the mixing of liquids at the interfacial boundary between channels is minimal, transferring a cell from the cell loading microchannel to the stimulus-containing reaction microchannel by negative dielectrophoresis corresponds to a complete and fully controlled medium exchange around the cell. Moreover, the microfluidic chip design allows to incubate cells with a stimulus solution for several minutes. For this purpose, the reaction microchannel is equipped with a delay loop (Figure 1B, C and Figure S3, Supporting Information), whose length together with the flow rate through the channel determine the total incubation time of a cell with the stimulus solution.

2.1.2. Custom Built Epifluorescence Microscope

The reaction microchannel of the FPFC is designed to wind backward and forward through the field of view of a microscope providing the means of optically quantifying cellular responses over time (Figure 1B, C). To encompass several microchannels in the field of view the custom built epifluorescence microscope used here is optimized for having a large field of view but is still capable of resolving single cells in flow. For this purpose a low magnification 20x microscope objective (Olympus, NA 0.9) is used to image the sample in conjunction with a fast CMOS camera (UI-3080CP Rev. 2, IDS) capable of acquiring at ≥50 frames per second and a sensor size to image at least five 30 μm microfluidic channels (Figure 1). The epifluorescence microscope is equipped with a 505 nm cut-on wavelength (DMLP505R Thorlabs) dichroic mirror and a 490 nm LED (M490L4 LED).

2.1.3. Real-Time Control Software

The main function of the control software is to track fluorescent cells in the microfluidic device. Given that cells repeatedly enter and leave the field of view when circulating in the reaction channel, the software cannot monitor what happens beyond the field of view, in the delay loop. Cells that are insufficiently separated from each other could overtake each other and disturb the cell sequence in the reaction channel. To prevent cells from swapping places in the flow, the transfer electrodes are actuated to move the next cell from the loading channel to the reaction channel only after the last transferred cell has moved sufficiently far downstream. To this end the LabVIEW written control software is programmed to activate the transfer electrodes ≥15 s apart which ensured a <1% swap rate in the reaction channel for a 90 s long delay loop. The control software excludes cell doublets, triplets or any other cell aggregates from transfer but also small fluorescent debris that can appear in the loading channels. This discrimination is achieved by selecting only cell like objects that are approximately circular (circularity >0.9) and using minimum/maximum area thresholds for selected objects. For tracking, the control software registers the position and the cumulative fluorescence intensity of the cells in several regions of interest (ROIs) in the field of view (**Figure 2**). The software generates a register for each ROI, that builds and clears as cells pass though, accounting for the position of the cells in the microfluidic device.

The software developed for the FPFC analyzer (Figure 1B) monitors a minimum of five ROIs (Figure 2B–D). The first region of interest (ROI1) is positioned in the cell loading microchannel immediately before the cell transfer electrodes and controls their operation (Figure 2A). ROI2 is situated in the reaction microchannel immediately after the electrodes. Because cells move slightly out of focus as a result of dielectrophoresis, the image data from ROI2 is not used as an initial fluorescence reading for the cell in the reaction microchannel and acts solely as a checkpoint for successful cell transfer. The third, fourth, and fifth regions of interest measure the cell fluorescence at specific locations within the delay loop (Figure 2A–D) providing information on the cellular fluorescence at three different time points during the incubation with the stimulus.

The software developed for the FPFC sorter controls an extra pair of electrodes (sorting electrodes) to sort cells of interest (Figures 1C and 2H). The software also monitors five ROIs within the field of view (Figure 2E–H). ROIs 1 and 2 have identical positions and functions as in the analyzer version of the code (Figure 2D). ROI3 is positioned at the end of the delay loop of the reaction microchannel, immediately before the sorting electrodes (Figure 2H). When a fluorescent cell is detected in ROI3, its fluorescence is recorded and compared to the fluorescence of the same cell in ROI1. If the fluorescence of the cell has increased by more than a certain specified threshold ratio, the software executes a decision to activate the sorting electrodes and transfer the responding cell from the reaction

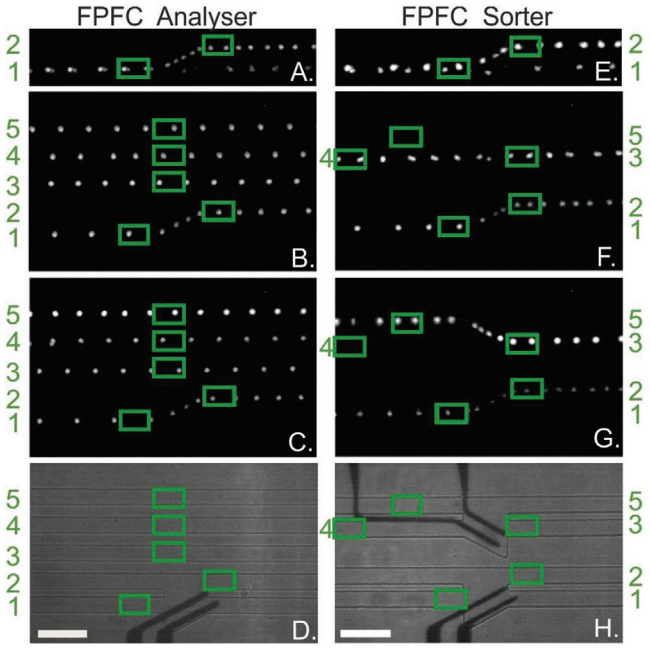

Figure 2. Superimposed images for a fluorescent cell travelling through the FPFC A–D) analyzer and E–H) sorter. Regions of interest (ROIs) are indicated by green boxes and ROI numbers are shown on the side of each image. A) Superimposed images illustrating the function of the transfer electrodes to move selected cells from the cell loading microchannel into the reaction microchannel of the FPFC analyzer. Typical flow paths of B) nonresponding and C) responding Ramos cells through the channels of the FPFC analyzer. D) A bright field picture of the imaging area of the FPFC analyzer showing the positions of ROIs with respect to the channels and electrodes within the microfluidic device. E) Superimposed images illustrating the function of the transfer electrodes to transfer only selected cells from the cell loading microchannel into the reaction microchannel of the FPFC sorter. Typical flow paths of F) nonresponding and G) responding Ramos cells through the channels of the FPFC sorter. H) A bright field picture of the imaging area of the FPFC sorter showing the positions of ROIs with respect to the channels and electrodes within the microfluidic device. The scale bars are of 100 µm in length.

microchannel into the cell collection microchannel. ROI5 provides a detection checkpoint for responding cells (Figure 2G). Nonresponders do not activate the sorting electrodes and are counted in ROI4 (Figure 2F).

2.2. Unaltered Intracellular Calcium Concentration of Ramos Cells after Dielectrophoresis

The stability of the intracellular calcium concentration of the Ramos cells in response to dielectrophoresis was demonstrated by performing control experiments, in which fluo-4 loaded Ramos cells in normal media were introduced to the cell loading microchannel and normal media were flown in the reaction microchannel of the FPFC analyzer (**Figure 3**A,C). Data for a total of 537 Ramos cells was collected during two control experiments carried out on different dates using separate microfluidic chips. Device run times were 2 h, and 2 h and 34 min with 240 and 297 cells, respectively, being evaluated during each run. The control experiments confirmed that in the absence of anti-BCR monoclonal antibody M15/8, the cumulative fluorescence of the Ramos cells does not change significantly during their time of travel along the reaction microchannel. An average fluorescence ratio (ratio of total fluorescence of a cell in ROI5 to total fluorescence of the same cell in ROI1) of 1.05 was observed over the two experiments. Only three cells (0.6%) out of 537 increased their fluorescence by more than 50% after dielectrophoresis (within 70, 72, and 77 s, respectively).

2.3. Evaluation of Intracellular Calcium Dynamics in Ramos Cells Exposed to the Anti-BCR Monoclonal Antibody M15/8 Using the FPFC Analyzer

In order to demonstrate and evaluate the time course of fluorescence response of Ramos cells to the anti-BCR monoclonal antibody M15/8, fluo-4 loaded Ramos cells in media were introduced into the cell loading microchannel and a 25 µg mL^{-1} solution of M15/8 in media was flown through the reaction microchannel of the FPFC analyzer. Data for a total of 625 Ramos cells were collected on four separate days using four different microfluidic chips (Figure 3B,D). 474 of the investigated

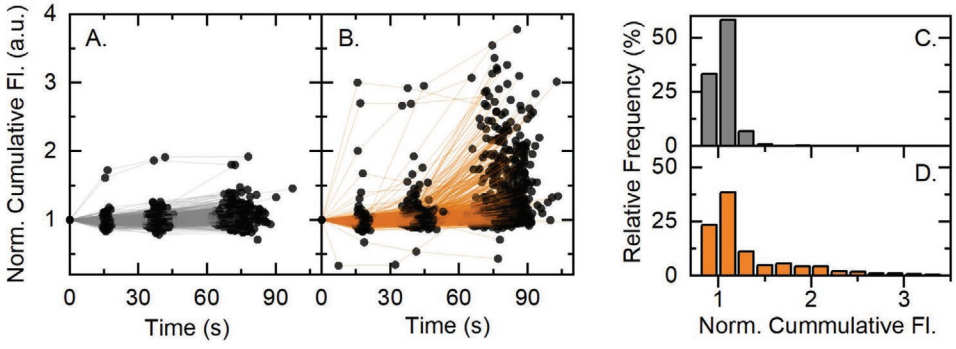

Figure 3. Studying the response of Ramos cells to antibody M15/8 in the FPFC analyzer. A) A plot of the total fluorescent pixel sum of 537 Ramos cells, each detected at three time points along the reaction microchannel of the FPFC analyzer in the absence of antibody M15/8 in two independent experiments. B) A plot of the total fluorescent pixel sum of 625 Ramos cells, each detected at three time points along the reaction microchannel of the FPFC analyzer in the presence of antibody M15/8 (25 µg mL^{-1}) in four independent experiments. C,D) Histogram showing the distribution of Ramos cells, which have attained a given fluorescence increase ratio in the C) absence and D) presence of antibody M15/8.

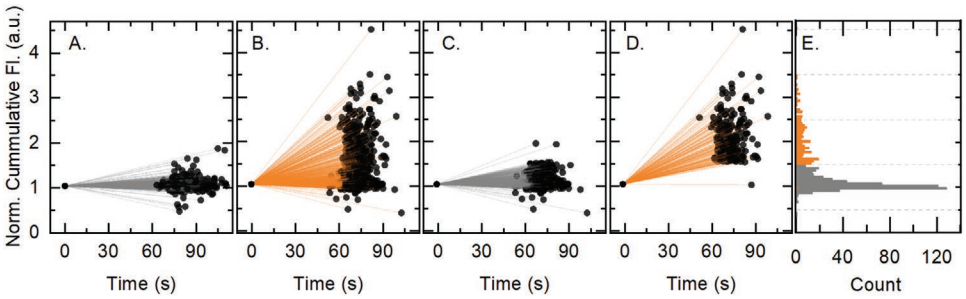

Figure 4. Sorting of Ramos cells according to their response to antibody M15/8 in the FPFC sorter. A) A plot showing the fluorescence increase ratio of 505 Ramos cells from control experiments performed with pure Ramos media flown through the reaction microchannel of the FPFC sorter in three independent experiments. B) A plot showing the fluorescence increase ratio of 753 Ramos cells incubated with 25 μg mL^{-1} of antibody M15/8 in the reaction microchannel of the FPFC sorter in three independent experiments. C,D) Plots showing the fluorescence increase ratio of sorted C) nonresponding and D) responding Ramos cells from the same data set as described in (B). E) Histogram of the fluorescence increase ratio for sorted nonresponders (gray) and responders (orange) from the same data set as described in (B).

cells did not show a significant increase in their total fluorescence after exposure to M15/8. The remaining 151 cells (24.2%) were classed as responders because they increased their fluorescence by more than 50% within 77 s of incubation (on average) with the antibody. The percentage of responding cells was found to be consistent between experiments with 22.4%, 24.1%, 24.0%, and 24.9% of responders having been identified during the four separate runs respectively and this remained stable over the entire experimental time (Figure S6, Supporting Information). Reacting cells exhibited fluorescence ratios in the range between 1.5 and 3.8 (Figure 3D). The majority of responders did not display a significant increase in fluorescence in ROIs 3 and 4 and reaction to the antibody only became evident in ROI5 (Figures 3B and 2C). This suggests that the downstream signaling cascade, which follows BCR ligation, does not result in a noticeable change of intracellular Ca^{2+} concentration until approximately at least 35 s after exposure of Ramos to the antibody.

2.4. Ramos Cell Sorting Based on the Intracellular Calcium Changes Generated by Their Exposure to the Anti-BCR Monoclonal Antibody M15/8 Using FPFC Sorter

As demonstrated with the FPFC analyzer, control experiments in the FPFC sorter confirmed that the intracellular calcium concentration of Ramos cells is not significantly affected by the dielectrophoresis conditions exerted by the cell transfer electrodes (**Figure 4**A). Fluo-4 loaded Ramos cells were introduced to the cell loading microchannel and pure Ramos media was flown through both the reaction and the cell collection microchannels. The control runs were carried out in triplicate on different days using separate microfluidic chips. An average fluorescence increase (ratio of total fluorescence of a cell in ROI3 to the total fluorescence of the same cell in ROI1) of 1.03 was observed over the three experiments. Four cells out of a total of 505 Ramos cells (0.8%) increased their total fluorescence by more than 50% when travelling along the reaction microchannel of the FPFC sorter (Figure 4A).

In cell sorting experiments fluo-4 loaded Ramos cells in media were introduced to the cell loading microchannel, a 25 μg mL^{-1} solution of antibody M15/8 in media was flown through the reaction microchannel and pure media was passed through the cell collection microchannel. Data for a total of 753 Ramos cells was collected on three separate days using a freshly prepared microfluidic chip each time (Figure 4B). The FPFC sorter was run for 67, 109, and 187 min, respectively, during each of the three experiments. As suggested by the control experiments a 1.5-fold increase in total fluorescence between ROI1 and ROI3 was chosen as a threshold and cells exhibiting a greater increase were classed as responders. 200 (26.6%) of the 753 cells were identified as responders and 197 of these were correctly sorted into the cell collection microchannel and detected in ROI5 (Figure 4D). The remaining 555 nonresponding cells did not activate the sorting electrodes and were detected and counted in ROI4 (Figure 4C). Two of the three cells not sorted despite >1.5-fold fluorescence increase remained in the reaction microchannel although the sorting electrodes were activated and were detected in ROI4 accounting as false negatives. The last of the three incorrect sorted cells (the outlier in Figure 4D) is a false positive that ended up in the collection channel even though the sorting electrodes did not activate. This is most likely due to a transient blockage in the reaction channel outlet, which briefly directed the flow through the inter-channel gap between the reaction microchannel and the sorting microchannel. With these errors as identified, the FPFC produces falls positives at a rate of 0.5% of the total population of cells of interest and false negatives at a rate of 1% of the total population of cells of interest. Nevertheless, using the post sort regions of interest ROI4 and ROI5 none of these errors goes undetected and any "contamination" can be quantified accurately.

3. Conclusion

The functional phenotype flow cytometer is an innovative microfluidic platform capable of sorting cells on the basis of their phenotypic responses. The FPFC performs a cascade of cell processing steps on a microfluidic platform. The FPFC exposes cells to a biological reagent (stimulus), incubates the cells with the stimulus, monitors cellular fluorescence and sorts the cells into subpopulations according to their

phenotypic responses to the stimulus to allow phenotypic cell sorting. Here we validate the FPFC by sorting cells according to their intracellular dynamics in response to an extracellular stimulus. As a natural extension this platform can also accommodate other types of cellular stimulation that could include intracellular stimuli to trigger intracellular cascades (e.g., via optical activation).

The design challenge for the FPFC is to perform the abovementioned steps in a microfluidic flow line. The main innovation of our design is the method of transferring cells between microfluidic channels through an inter-channel gap. Several design advantages are associated with this method. Firstly the arrangement allows for the cell to be transferred from one environment to another accounting for a change in the extracellular media—in flow. Secondly the cell can be incubated for minutes in the new extracellular environment. This is made possible since the transfer can be activated on demand to shuttle cells between channels at arbitrary time points and hence introduce sufficient spacing between the cells. Sufficient spacing between cells in the reaction microchannel of the device prevents cells swapping positions in flow and allows for reliable cell tracking. Previous attempts to space cells in microfluidic channels employed 3D focusing flow.[14] In contrast to the inter-channel gap transfer developed here, the 3D focusing method cannot be activated on demand. Hence the final inter-cell spacing achieved with the 3D focusing will depend on the initial inter-cell spacing, which cannot be well controlled. This limits the precise assignment of inter-cell gaps and generates assignment errors limiting the incubation time to a few seconds. Hence using the inter-channel gap method allows for precise cell assignment control and long incubation times that extend over minutes as demonstrated here. Nevertheless, the desired accuracy of cell tracking dictates the throughput of the device which is currently reached at a maximum of 4 cells min^{-1} but can be further improved by minimizing the variability of cell speeds in the flow channels, for example by coating the microfluidic channel cell surface with a nonstick substrate that minimizes cell-wall interactions.[21]

Another important aspect of our design is the presence of a delay loop in which cells, in flow, are kept once the extracellular environment has been changed. The delay loop in combination with the ability to control the transfer of cells into the delay loop allow for incubation times that scale proportional to the length of the delay loop and inversely proportional to the flow speed. Nevertheless, the stability of the flow and cell sedimentation must be considered when lowering the flow speed and the increased hydraulic pressure associated with the increased channel length must be considered when extending the incubation time in the FPFC. Our calculations, predict that feasible incubation times for the FPFC, driven at 50 mBar input pressure, can reach 15 min with a throughput of 1 cell per 2 min.

In the current implementation of the FPFC we chose negative dielectrophoresis as a cell transfer method between the inter-channel gap. We have demonstrated that the conditions of negative dielectrophoresis do not cause any significant undesired electrical disturbance to the cells and the intracellular calcium concentration of Ramos cells remains sufficiently stable for the duration of their travel in the reaction microchannel of the device during control experiments. The average diameter of the Ramos cells, dislocated by dielectrophoresis, is of 19 ± 2 μm with a minimum diameter of 13 μm and a maximum diameter of 23 μm. It is to be expected that negative dielectrophoresis in the FPFC will work for other cell types with similar sizes, but in any case, alternative methods of moving cells between channels could be adopted if cells are sensitive to electrical perturbation.

Similar to flow cytometry, two versions of the FPFC have been described here: the FPFC analyzer and the FPFC sorter. The FPFC analyzer samples 4 time points of the intracellular kinetics curve whereas the FPFC sorter samples only 2, making the analyzer a potentially useful tool for informing the best time delay to be used in the sorter. In the future, both the number of time points in the analyzer and sorter could be further increased, for example by increasing the camera sensor size or reducing the microscope magnification to 10x. The analyzer will generally be able to accommodate more points on the kinetics curve since it can use chip space used otherwise for sorting for further sampling. In both designs the total incubation time with the stimulus and the time intervals between data points can be changed by adjusting the total length of the reaction microchannel and the length of individual delay loops between consecutive crossover points of the reaction microchannel with the imaging area respectively.

Using the FPFC analyzer we have concluded that an increase in total fluorescence of >1.5-fold can be used to sort Ramos cells according to their response to the anti-BCR monoclonal antibody M15/8. The 1.5 threshold has been chosen to minimize false positive cells as demonstrated in our control experiments. In other experiments, the criterion for distinguishing between responding and nonresponding cells may need to be adjusted in the search for a biologically meaningful distinction between the segregated cell subpopulations.

The functional cell sorting technology described here opens a gateway for further in-depth investigation of the links between cellular phenotype and the profiles of different cell omic layers.[6] For example, sorted subpopulations of responding and nonresponding Ramos cells can be harvested and analyzed for differences in the expression levels of the proteins implicated in the signaling cascade, which follows BCR ligation. In such experiments the cell collection channel of the microfluidic chip could be loaded with a reagent such as an RNA stabilizing solution (e.g. RNAlater) in order to preserve the RNA of the Ramos cells at the levels observed during sorting for subsequent RNA sequencing and analysis.

We further envisage potential uses of our technology in the fields of functional peptide screening,[22,23] RNA interference[24] and CRISPR/Cas9[25] based cell screening. With all these potential applications in mind we anticipate that the FPFC will be an important new technology in studying the biological significance of the heterogeneity of cellular subpopulations as well as in deciphering the biochemical mechanisms underlying the phenotypic responses of cells to extracellular stimuli.

4. Experimental Section

Microfluidic Chip Fabrication: The technical drawings for the microfluidic channel designs were drawn using DraftSight 2018 software

and sent to Micro Lithography Services (UK) for the printing of film photomasks of the microfluidic channels (Figures S1 and S3, Supporting Information). An SU-8 (an epoxide-based negative photoresist) mold of the microfluidic channels was prepared on a silicon wafer substrate from the film photomask using standard photolithography techniques. Polydimethylsiloxane (PDMS) elastomer was then poured and set onto the SU-8 master mold. PDMS slabs containing the microchannels were cut out of the master mold and holes were punched at the channel inlets and outlets.

Metal electrodes were deposited onto glass microscopy slides using photolithography, metal sputter coating, and lift-off techniques (Figures S2 and S4, Supporting Information). A glass microscopy slide (#1.5; 24 × 50 mm) was initially coated with a 3 µm thick uniform layer of AZ photoresist (AZ nLOF 2035, MicroChemicals GmbH, Germany). The electrode pattern was then formed in the AZ photoresist using photolithography followed by chemical development. A layer of Au/Pd (1:4, 50 nm) was deposited using a sputter coating instrument on the side of the microscopy slide containing the electrode pattern and this was followed by a lift-off process in acetone to obtain the metal electrodes on the glass slide substrate.

The PDMS microchannels and the glass microscopy slide with the metal electrodes were treated with oxygen plasma and bonded together under a microscope to carefully align the metal electrodes across the interchannel gap. Finally, copper wires (≈5 cm long) were glued to the electrode ends of the microfluidic chip using silver conductive epoxy adhesive (cat. no.: 186–3616, RS components Ltd., UK) followed by incubation at 70 °C for 1 h.

Software: LabVIEW 18.0f2 is used for acquiring and analyzing images in real-time and activating the transfer and the sorting electrodes. The software defines rectangular regions of interest (ROIs) within the imaging area of the digital camera. Ramos cells passing through the ROIs were detected as fluorescent particles using a 30 a.u. intensity threshold. Individual particle pixels were corrected against a dark background calculated as the average value of all nonparticle pixels. No correction was applied for the variance in illumination since this was smaller than 1% across the field of view. A minimal pixel area threshold of 1000 square pixels was used as a filter for cell debris. The total fluorescence pixel sum of cells was calculated as the sum of all particle pixels (dark background corrected). The total fluorescence pixel sum of cells at the beginning and the end of the delay loop of the reaction microchannel of the FPFC sorter were stored in arrays, whose indices were related to the order in which the cells flow through the channel. The LabVIEW code executes a decision to turn on the sorting pair of electrodes on the basis of the comparison of the initial and final fluorescence values of each individual cell from the arrays associated with the relevant ROIs.

Ramos Cell Culture Maintenance: Ramos cell culture was grown in T75 tissue culture flasks with hydrophobic surface, canted neck, and vented cap (cat. no.: 83.3911.502, Sarstedt Ltd.). Culture media was prepared using RPMI 1640 media (cat. no.: 11531851, Fisher Scientific) with heat inactivated fetal bovine serum (10% v/v; cat. no.: 10500064, Thermo Fisher Scientific), penicillin-streptomycin (1% v/v; cat. no.: 11528876, Fisher Scientific), 200×10^{-3} M L-glutamine (1% v/v; cat. no.: 11500626, Fisher Scientific), 100×10^{-3} M sodium pyruvate (1% v/v; cat. no.: 12539059, Fisher Scientific), and 50×10^{-3} M 2-mercaptoethanol (0.1% v/v; cat. no.: 31350010, Thermo Fisher Scientific). Confluent cell culture was diluted with fresh media by a factor of 10 every other day and by a factor of ≈20 prior to weekends up to a final volume of ≈11 mL per flask.

Loading of Ramos Cells with Fluo-4, AM:[26] Confluent culture of Ramos cells (2 mL) was centrifuged (1000 rpm, 5 min) in a 15 mL falcon tube. The supernatant was carefully decanted, fresh media (2 mL) was added, and the pellet was carefully resuspended by trituration with a suction pipette. Fluo-4, AM (Thermo Fisher Scientific) in dimethyl sulfoxide (5 µL, 4.6 µmol) was added and mixed well with the Gilson pipette. The Ramos cell suspension was carefully transferred to a T25 tissue culture flask with hydrophobic surface and incubated at 37 °C, 5% CO_2 for 45 min. The fluo-4 loaded cells were then transferred back to a 15 mL falcon tube and centrifuged (1000 rpm, 3.5 min). The supernatant was carefully decanted and fresh media (0.2–1.0 mL) was added to give a final cell count of less than 10^5 Ramos cells per milliliter. A test experiment probing the viability of the cells was performed in bulk with cells being let to sediment and then slowly exposed to the M15/8 antibody. Demonstrating their viability cells have increased their fluorescence as shown in Figure S5 (Supporting Information).

Experimental Setup: Microfluidic chips were primed using a Fluigent MFCS-EZ Microfluidic flow control system. The channel inlets were loaded by inserting Gilson pipette tips containing 40 µL of solution or homogeneously suspended cell suspension into the holes of the channel inlets. A primed and loaded microfluidic chip was mounted and secured on the stage of the epifluorescence microscope (Figure S7, Supporting Information), so that the imaging area of the digital camera captured approximately the correct imaging area of the chip for the FPFC analyzer and FRPF sorter instruments (Figure 1B,C). The copper wires of the FPFC analyzer were connected to the output channel of a function/pulse generator (TGF3162, Thurlby Thandar) using test leads (IN04467, Combined Precision Components). In order to run the FPFC in sorting mode, the copper wires of a sorter chip were connected to the output channels of two separate function/pulse generators. The TGF3162 instruments were set to generate a voltage of 9 Vpp at a frequency of 800 kHz on external trigger of +5V (DC). The external trigger channels of the TGF3162 instruments were connected to separate analogue voltage output channels of a multifunction input/output DAQ device (USB-6002, National Instruments) connected to the control PC via a USB 3.0 port.

Statistical Analysis: The data presented in Figure S6 (Supporting Information) included statistical analysis which was presented as mean ± SD. A minimum of four different experiments were used for calculating the mean. All the conditions were statistically evaluated by one-way analysis of variance (ANOVA) with *t*-test ($p < 0.05$) run in Prism 9.0.0.

Supporting Information

Supporting Information is available from the Wiley Online Library or from the author.

Acknowledgements

C.C., P.N., C.S., and F.G. would like to thank the BBSRC BB/R022127/1 for providing funding to support this work. C.C. would also like to thank the Academy of Medical Sciences Springboard Award for providing support for this work. R.C. is funded by SNF CRSK-3_190550.

Conflict of Interest

C.C., P.N., C.S., and F.G. are inventors on patent application GB2018910.6.

Data Availability Statement

Research data are not shared.

Keywords

calcium, cell sorting, phenotypes, real time, time domain

Received: January 26, 2021
Revised: May 21, 2021
Published online: June 23, 2021

[1] N. Nitta, T. Sugimura, A. Isozaki, H. Mikami, K. Hiraki, S. Sakuma, T. Iino, F. Arai, T. Endo, Y. Fujiwaki, H. Fukuzawa, M. Hase, T. Hayakawa, K. Hiramatsu, Y. Hoshino, M. Inaba, T. Ito, H. Karakawa, Y. Kasai, K. Koizumi, S. W. Lee, C. Lei, M. Li, T. Maeno, S. Matsusaka, D. Murakami, A. Nakagawa, Y. Oguchi, M. Oikawa, T. Ota, K. Shiba, H. Shintaku, Y. Shirasaki, K. Suga, Y. Suzuki, N. Suzuki, Y. Tanaka, H. Tezuka, C. Toyokawa, Y. Yalikun, M. Yamada, M. Yamagishi, T. Yamano, A. Yasumoto, Y. Yatomi, M. Yazawa, D. Di Carlo, Y. Hosokawa, S. Uemura, Y. Ozeki, K. Goda, *Cell* **2018**, *175*, 266.
[2] M. Labib, S. O. Kelley, *Nat. Rev. Chem.* **2020**, *4*, 143.
[3] S. J. Altschuler, L. F. Wu, *Cell* **2010**, *141*, 559.
[4] D. Muzzey, A. van Oudenaarden, *Annu. Rev. Cell Dev. Biol.* **2009**, *25*, 301.
[5] M. J. Sanderson, I. Smith, I. Parker, M. D. Bootman, *Cold Spring Harbor Protoc.***2014**, *2014*, 1042.
[6] L. Chappell, A. J. C. Russell, T. Voet, *Annu. Rev. Genomics Hum. Genet.* **2018**, *19*, 15.
[7] Z. Környei, S. Beke, T. Mihálffy, M. Jelitai, K. J. Kovács, Z. Szabó, B. Szabó, *Sci. Rep.* **2013**, *3*, 1088.
[8] J. Lee, Z. Liu, P. H. Suzuki, J. F. Ahrens, S. Lai, X. Lu, S. Guan, F. St-Pierre, *Sci. Adv.* **2020**, *6*, eabb7438.
[9] B. Chen, S. Lim, A. Kannan, S. C. Alford, F. Sunden, D. Herschlag, I. K. Dimov, T. M. Baer, J. R. Cochran, *Nat. Chem. Biol.* **2016**, *12*, 76.
[10] C. Brasko, K. Smith, C. Molnar, N. Farago, L. Hegedus, A. Balind, T. Balassa, A. Szkalisity, F. Sukosd, K. Kocsis, B. Balint, L. Paavolainen, M. Z. Enyedi, I. Nagi, L. G. Puskas, L. Haracska, G. Tamas, P. Horvath, *Nat. Commun.* **2018**, *9*, 226.
[11] A. Gross, J. Schoendube, S. Zimmermann, M. Steeb, R. Zengerle, P. Koltay, *Int. J. Mol. Sci.* **2015**, *16*, 16897.
[12] D. Basiji, M. R. O'Gorman, *J. Immunol. Methods* **2015**, *423*, 1.
[13] H. Mikami, M. Kawaguchi, C. J. Huang, H. Matsumura, T. Sugimura, K. Huang, C. Lei, S. Ueno, T. Miura, T. Ito, K. Nagasawa, T. Maeno, H. Watarai, M. Yamagishi, S. Uemura, S. Ohnuki, Y. Ohya, H. Kurokawa, S. Matsusaka, C. W. Sun, Y. Ozeki, K. Goda, *Nat. Commun.* **2020**, *11*, 1162.
[14] Y. Zhao, W. Zhang, Y. Zhao, R. E. Campbell, D. J. Harrison, *Lab Chip* **2019**, *19*, 3880.
[15] X. Z. Jiang, H. Toyota, T. Yoshimoto, E. Takada, H. Asakura, J. Mizuguchi, *Apoptosis* **2003**, *8*, 509.
[16] S. An, K. A. Knox, *FEBS Lett.* **1996**, *386*, 115.
[17] C. A. Walshe, S. A. Beers, R. R. French, C. H. Chan, P. W. Johnson, G. K. Packham, M. J. Glennie, M. S. Cragg, *J. Biol. Chem.* **2008**, *283*, 16971.
[18] V. Rolli, M. Gallwitz, T. Wossning, A. Flemming, W. W. Schamel, C. Zurn, M. Reth, *Mol. Cell* **2002**, *10*, 1057.
[19] Y. Kulathu, E. Hobeika, G. Turchinovich, M. Reth, *EMBO J.* **2008**, *27*, 1333.
[20] U. Seger, S. Gawad, R. Johann, A. Bertsch, P. Renaud, *Lab Chip* **2004**, *4*, 148.
[21] R. A. Kellogg, R. Gómez-Sjöberg, A. A. Leyrat, S. Tay, *Nat. Protoc.* **2014**, *9*, 1713.
[22] P. E. Saw, E. W. Song, *Protein Cell* **2019**, *10*, 787.
[23] S. Ahmed, A. S. Mathews, N. Byeon, A. Lavasanifar, K. Kaur, *Anal. Chem.* **2010**, *82*, 7533.
[24] S. Gao, C. Yang, S. Jiang, X. N. Xu, X. Lu, Y. W. He, A. Cheung, H. Wang, *Protein Cell* **2014**, *5*, 805.
[25] J. Kweon, Y. Kim, *Arch. Pharm. Res.* **2018**, *41*, 875.
[26] K. R. Gee, K. A. Brown, W. N. Chen, J. Bishop-Stewart, D. Gray, I Johnson, *Cell Calcium* **2000**, *27*, 97.